PCCP

Laser pulses into bullets: Tabletop shock experiments

Journal:	*Physical Chemistry Chemical Physics*
Manuscript ID	CP-PER-01-2022-000418.R1
Article Type:	Perspective
Date Submitted by the Author:	20-Mar-2022
Complete List of Authors:	Dlott, Dana; University of Illinois at Urbana-Champaign College of Liberal Arts and Sciences, School of Chemical Sciences

Laser pulses into bullets: Tabletop shock experiments

Dana D. Dlott*

School of Chemical Sciences and Fredrick Seitz Materials Research Laboratory

University of Illinois at Urbana-Champaign, Box 01-6 CLSL, 600 S. Mathews Ave., Urbana, IL 61801 USA

Abstract

This article discusses tabletop high-throughput laser experiments on shock waves in solids and liquids, where the more usual laser pump pulse is replaced by a 0.5 mm diameter laser-launched bullet, a thin metal disk called a flyer plate. The hypervelocity flyer (up to 6 km/s or Mach 18) can have kinetic energy (~1J) to briefly produce extreme conditions of temperature and pressure, thousands of K and tens of GPa (1 GPa = 10,000 bar) in a small volume with a rise time <2 ns. The experiments are performed using a "shock compression microscope", a microscope fitted with the laser flyer launcher plus an optical velocimeter, a high-speed laser interferometer that measures the motion of the flyer plate or the sample material after impact. This makes it possible to generate extreme conditions at the push of a button in an intrinsically safe environment, and probe with any of the diagnostics used in microscope experiments, such as high-speed video, optical emission, nonlinear coherent spectroscopies and so on. The barrier to entering this field is relatively low since many laser laboratories already possess much of the needed instrumentation. A brief introduction to shock waves and instrumentation is presented. Then several examples of recent applications are described, including shocked water, the photophysics of fluorescent molecules under extreme conditions, shocked protein solutions, shocked metal-organic frameworks (MOFs), shocked explosives, chemical catalysis in a shocked

* Corresponding author. Electronic mail dlott@illinois.edu.

liquid, and molecules at shocked interfaces. Since one can shoot a bullet at practically anything, there are many emerging opportunities in chemistry, biophysics, materials science, physics and hypervelocity aerodynamics.

1. Introduction

The readers of this Journal are undoubtably familiar with experiments where a sample is excited with a short laser pulse to time resolve the dynamics of electronic or vibrational states. I have spent many decades developing and using ultrafast nonlinear and coherent spectroscopies to study molecular solids, liquids and interfaces. Often a nonlinear signal was too weak so we increased the laser pulse energy, but instead of getting a bigger signal we got sample damage and sometimes laser ablation, and I became interested in material damage and shock waves. In 1988 I attended an Army Research Office sponsored symposium on shock waves, explosives and propellants where I was introduced to research in those areas. I was invited because I had done experiments on vibrational relaxation in solids[1] and liquids,[2] and vibrational energy dynamics had begun to be a topic of interest in that community.[3, 4] The symposium inspired me and my colleague (and former PhD advisor) Prof. Michael Fayer to develop a theory of multiphonon up-pumping in explosives,[5-7] which describes shock initiation of chemical reactions in energetic materials (EM) by chemically-significant levels of vibrational excitation produced from a dense bath of phonons excited by shock waves. This theoretical modeling inspired me to begin experimental studies in this area.

I will not attempt to summarize the current and prior state of research in shocked materials. The American Physical Society Topical Group on Shock Compression in Condensed Matter (GSCCM) has a biennial meeting where hundreds of researchers present papers that are collated in conference proceedings, lately by the American Institute of Physics, where interested readers can become acquainted with this field.[8] Classical experiments were focused on shock waves generated by guns that accelerate disk-shaped projectiles called “flyer plates” to high velocities, or explosives, and now kilojoule lasers, that produce steady planar material flows

lasting hundreds of nanoseconds or microseconds.[9] The material flow and shock waves were probed by velocity measurements, and sometimes by spectroscopy.

Such experiments, typically performed by research teams at large government research laboratories, stand in stark contrast to typical tabletop ultrafast laser experiments done at high repetition rates, often by a single person who did not need to be barricaded in a bunker for safety. I thought there was an opportunity to adapt ultrafast spectroscopy methods to investigate the short time and length scale phenomena that underlie the macroscale phenomena of high-velocity impacts and detonations.

It is actually not difficult for an ultrafast spectroscopy laboratory to do shock experiments. One common method, called the confined ablation technique, is to deposit a thin absorbing layer such as a metal film, on a window in contact with the test sample and use a laser pulse to ablate the film to drive a shock into the sample.[10] Because laser pulses can be focused to a small spot, this method can produce high pressures, but the resulting shocks do not remain planar or persist for very long.

Although my group has made use of confined ablation in many applications,[11, 12] over the past decade we have developed another method where experiments are done in a tabletop microscope, called a "shock compression microscope".[13, 14] It uses a Q-switched Nd:YAG laser to launch 0.5 mm diameter flyer plates[15-17] at velocities up to 6 km/s or Mach 18 (Mach 1 = 0.331 km/s) and optical velocimeter. Various optical diagnostics can be used to probe solid and liquid dynamics with micrometer spatial and nanosecond time resolution. In this Perspective I will describe the fundamentals of this method, which turns laser pulses into hypervelocity bullets, describe some recent applications, and conclude with suggestions for further work in this

area, which is now developing rapidly. After all, one can shoot a bullet at practically anything, solid, liquid, gas, plasma, but perhaps not dark matter(!).

Tabletop shock wave spectroscopy is not just ultrafast spectroscopy with bullets instead of laser pulses. There are profound differences that will be discussed here. Shock experiments are destructive, so instead of using many laser pulses on a single sample, we use many identical samples, each with a single shock. Laser pulses can excite a sample in femtoseconds, but shocks propagate 10^5 times slower than light, so the time for a shock to excite a sample is limited by the time for the shock to traverse the sample. Shocks in condensed matter move at kilometers per second, and it is useful to keep the following relations in mind:

1 km/s = 1 mm/μs = 1 μm/ns = 1 nm/ps.

To get picosecond time resolution the sample has to be nanometers thick,[11] and to get nanosecond time resolution the sample has to be micrometers thick.[18, 19] Femtosecond laser pulses are ideally δ-functions, but flyer plate shocks are step functions where the duration is determined by the flyer plate thickness. Our 12-100 μm thick flyers produce shocks lasting 2-20 ns, although the thicker, heavier flyers have lower top speed.[16] The flyer plate is launched with laser pulses lasting tens of nanoseconds, but the shock risetime can be far faster. We have observed rise times <0.5 ns,[20] but <2 ns is more typical. Actually, the risetime is determined by the flatness and parallelism of the plate-target impact and could be picoseconds. Flyer plates can impart vastly more energy to a sample than femtosecond pulses, since high-energy femtosecond pulses interact primarily with electrons and produce massive ionization, whereas regardless of the pulse energy used to launch the flyer, the flyer interacts solely with external mechanical degrees of freedom. Our flyer plates, with kinetic energies in the Joule range, can briefly create

extreme conditions of temperature (thousands of K) and pressure (tens of GPa), where the energy density associated with 1 GPa is 10^9 J/cm^3, and the pressure 10,000 bar.

2. Shock waves for dummies

"What is a shock wave?" is illustrated in Fig. 1a for a planar impact with a material initially at density ρ_0.[21] If the flyer velocity v is low (Fig. 1b), it launches an acoustic pulse, a superposition of acoustic phonons which disperses as it propagates. A shock wave is produced when the flyer velocity is fast enough to cause the flyer/sample interface to move at a material velocity designated U_p (the "p" is archaic, it refers to the "plate" velocity). As illustrated in Fig. 1c, the material motion leads to a higher-density region behind the shock front that is irreversibly heated by adiabatic compression. The shock velocity U_s is roughly $U_p + c_0$, where c_0 is the speed of sound.[22]

Shock waves are nonlinear excitations that can steepen up,[23] as illustrated in Figs. 1d,e. The finite rise in Fig. 1d can be viewed as a lower-pressure, slower-moving leading shock and a higher-pressure, faster-moving trailing shock. Hence the shock tends to steepen up (Fig. 1e). In a hypothetical elastic medium the shock front is a discontinuity, but in real media the shock front rise is finite.[23] Processes that transform the directed energy of the shock into transverse or random energies are collectively called "shock viscosity",[24] the large-amplitude version of traditional viscosity.

The steepest shocks are observed in thin layers of stiff materials and the shock duration tends to increase with propagation distance. The steepest shocks observed so far were in sapphire. The rise time was 1.2 ps and the velocity about 11 km/s = 11 nm/ps.[25] So this shock front was ~13 nm in width. In a molecular self-assembled monolayer the rise time was 4 ps.[11] In an Al thin film the rise time was 20 ps.[26, 27] In a 700 nm thick pressed polycrystalline

anthracene layer the shock front was <25 ps.[19] In a 1 cm thick slab of polycrystalline Al the rise time was hundreds of nanoseconds.[24]

Early shock experiments were primarily reliant on velocity measurements.[22] These can be used to determine a shock equation of state termed the Hugoniot, which is typically expressed as U_s versus U_p. The Rankine-Hugoniot relations, which assume conservation of mass, momentum and energy, show that the pressure (the rate of momentum flow per unit area) of a material with initial density ρ_0 can be determined knowing velocities U_s and U_p,[22]

$$P = \rho_0 U_s U_p, \quad (1)$$

which is why shock waves are the primary pressure standard for high pressures.

The Hugoniot equation of state gives pressures and densities from velocities but it says nothing about temperature, and temperature determinations are a continuing problem in shock compression science. The temperature rise can be described as,

$$T_1 = T_0 e^{-\Gamma \Delta V} + \Delta T_{irr},^{23} \quad (2)$$

where ΔV is the specific volume change, ΔT_{irr} is the temperature increase above and beyond a reversible adiabatic compression, which depends on the path, and Γ is the Grüneisen parameter. The path that produces the largest ΔT_{irr} and the highest temperature is the single-stage shock.

3. Getting calibrated

To get calibrated to the effects of flyer plate impacts, we consider shocks in water,[28-34] as shown in Fig. 2. Keep in mind that as in all aspects, water is a special case. It is a low-density hydrogen-bonded liquid more compressible that most other liquids, and unlike most other liquids, water expands when it freezes. So shocking water favors phase transitions in various forms of ice which is offset by shock heating. Since water is so compressible, the temperatures in Fig. 2 are relatively high, and it is believed that shocked water is always liquid. With more

gradual, more nearly reversible compression, where $\Delta T_{irr} \approx 0$, water does freeze into phases such as IceVII.[33-35]

Figure 2 shows computed pressure and temperature versus flyer plate impact velocity, where we consider that only a fraction of the flyer plate kinetic energy is transferred to the water due to shock impedance mismatch. Figure 2 shows that with a 5 km/s flyer plate launcher the peak pressure will be 27 GPa (1 GPa = 10,000 atm) and the temperature 2200K.

Shock compression tends to polarize neutral media, and in water it facilitates proton transfer, since ion pairs have a higher density than hydrogen-bonded molecules. With ambient water, pH = 7, pOH = 7 and pKw = 14, and $[H^+]$ is 10^{-7}M. Water can be shocked into a fully-ionized state of superionic liquid,[36, 37] so shock waves can convert liquid water from a hydrogen-bonded liquid into a molten salt H^+OH^-.

4. Shock compression microscope

Our shock compression microscope, depicted in Fig. 3a, consists of an inverted microscope fitted with laser flyer launcher and optical velocimeter.[13] In the inverted configuration the sample lies flat on the microscope stage which is useful for loose powders and liquids. The laser is a multimode Q-switched Nd:YAG that produces 10 ns duration 2.5 J pulses. The key to achieving a planar reproducible launch is to spatially homogenize the laser beam, as described previously.[15-17]

We use a fiberoptic photon Doppler velocimeter (PDV)[38, 39] described in Fig. 4. It is a fiberoptic interferometer with a single-mode 1.55 μm laser diode. As the target material moves, a beat pattern is detected. Knowing the laser wavelength and beat frequency, the time-dependent velocity profile can be determined. Figure 4 shows a configuration with a window target that

measures the flyer velocity. When the flyer impacts the window, PDV measures the flyer/window interface velocity.

Figure 5 shows some results obtained using PDV that illustrate the range of flyer velocities and velocity reproducibility. Figure 5a shows velocities of Al and Cu flyers of different thicknesses as a function of launch laser fluence. Figure 5b shows a reproducibility test where 33 flyers were shot from 25 μm thick Al. The velocity variance was less than 1%, and most of the variance was due to two shots that were slightly slower than the others.

Since shock experiments are inherently destructive, we have developed methods for fabricating multielement target arrays, as described in Fig. 3b. The 0.5 mm in diameter flyer plates are launched from metal foil cemented to a glass window with low-viscosity epoxy. A 50 x 50 mm^2 window can be used to launch hundreds of flyer plates. The flyer plate travels across a 0.375 mm vacuum gap before impacting the target. The gap allows time for the flyer to accelerate to its peak velocity.[16]

Three sample configurations are illustrated in Figs. 3b,c,d. In Fig. 3b the sample is a coating on a window. The optional thin-layer mirror allows the velocimeter to observe the velocity profile produced by the shock exiting the sample into the window. In Fig. 3c a Kapton adhesive tape with an array of holes on a glass window forms an array of wells formed by the holes and window which can be filled with solid materials.[40] Figure 3d is the same as Fig. 3c except the sample is liquid. An array of 50 microcuvettes can be made by filling the wells with liquid and covering them with a thin lid that is impedance-matched with the flyer plate.[41] We typically use Al foils for the flyers and 9 μm thick Al foil for the lids. The lid is thin enough to transmit the shock from the flyer plate but thick enough to get a good seal on the liquid.

Since the sample is mounted on a microscope it is possible to use many different kinds of optical probes to study the shocked sample, although detectors that acquire large data sets on a single shot are favored. Some samples produce their own emission during an impact. Otherwise we can illuminate with a light-emitting diode, a Xe flashlamp, a 250 ns green or UV pulse, or a femtosecond strobe. For detectors we use a nanosecond camera, which consists of several 3 ns gated intensified charge-couple devices (Specialised Imaging SIMX) which, together with the microscope optic gives 2 μm spatial resolution, a streak camera or a homebuilt streak camera consisting of a high-throughput prism spectrograph with 32 fiber optics in the image plane leading to 32 fast photomultipliers and digitizers. This spectrograph measures spectral radiance from 450-825 nm every 0.8 ns, and it can function as a 32-channel optical pyrometer to determine time-dependent temperature profiles.[42]

5. Photoemissive probes

Photoemissive probes such as organic dyes or quantum dots allow shock effects to be visualized in real time at specific locations where the probe is bound.[43] For example, a planar shock in a microstructured medium develops a complex spatial profile where the pressure can be very different at different locations.

Photoemissive probes in polymer coatings are used as "pressure-sensitive paint"[44-46] (PSP) to visualize air flows. PSP consists of an oxygen-sensitive emissive probe suspended in an oxygen-permeable binder.[44, 45] When the oxygen partial pressure changes, the emission quenching due to enhanced intersystem crossing changes correspondingly. That allows, for example, visualization of a complex atmospheric flow field over a vehicle surface at video frame rates. The time response of PSP is ordinarily limited by the rate oxygen diffuses into the paint,

so it is rather slow. The fastest response uses nanoporous paint to facilitate oxygen diffusion, and response times were achieved as low as 2 μs.[44]

In condensed phase shock experiments the pressure is vastly greater, enough to produce bulk compression of the PSP, and nanosecond time response is needed. In order to understand how to achieve such a fast PSP response, we need to understand the photophysics that cause the emission frequency to shift and the intensity to change.

The results shown here use Rhodamine 6G (R6G) dye in poly-methyl methacrylate (PMMA) illuminated by a green laser pulse.[47, 48] A 3-level Jablonski diagram to describe the effects of high pressure on photoemission is shown in Fig. 6.[47] The emission shift, which is typically a redshift, is a solvation effect resulting from the shock density increase. When a dye is dissolved in a medium, the ground state energy (state 1 in Fig. 5) decreases. The energy of the singlet excited state (state 3 in Fig. 6), which is more polarizable, decreases even more, resulting in an emission redshift. This shift is an essentially instantaneous response to changes in the local environment.

Emission intensity and lifetime decreases result from an enhancement of nonradiative relaxations, principally enhanced intersystem crossing, although enhanced internal conversion is also a factor. Increased density lowers state 3 energy and raises the triplet state 2. Density increases the triplet state energy because the parallel spins resist being driven closer together. The net result is a decrease in the singlet-triplet splitting and increased intersystem crossing to the dark triplet state.[49]

Figure 7 shows results from 2 mM R6G in PMMA with an impact from a 100 μm thick flyer plate at 1.1 km/s, producing a 4 GPa shock that lasts about 15 ns.[47] Figure 7a is the time-dependent emission spectra showing intensity loss and redshift. The intensity loss is computed

as the fractional change in area under the emission peak and the redshift as the first moment of the spectrum (the average emission wavelength). As shown in Fig. 7b, the redshift peaks at the end of the shock and then decays. The intensity loss in Fig. 7c also increases during the shock, and the intensity loss is long-lived. Figure 7d shows that the redshift risetime is about 7 ns faster than the intensity loss.

The redshift does not recover fully at longer times because the polymer undergoes plastic deformation that permanently densifies the shocked region. The intensity loss lags behind the redshift because of the time needed for intersystem crossing into the dark triplet state.[47]

Absolute intensity measurements of the pressure distribution within a PSP in a shocked material can be problematic because the emissivity can change when the material moves or begins to develop cracks or other damage. One way to overcome problems associated with absolute intensity measurements is fluorescence lifetime imaging,[50] since the lifetime is insensitive to changes in the emissivity. To measure the lifetime during a shock, the sample is irradiated by a short-duration pulse while the radiative decay is measured with a fast photodetector or streak camera.[51]

Figure 8 shows a measurement of the fluorescence decay of R6G in PMMA.[51] R6G is excited by a femtosecond pulse and the decay is measured with a 50 ps streak camera. The shock duration of 15 ns is longer than the ambient fluorescence lifetime of 3.3 ns (Fig. 8) so the R6G is subject to a high pressure that remains constant during the decay. When the R6G is shocked, the lifetime decreases, as shown in Fig. 8a, due to increased nonradiative relaxation. Figure 8b shows the lifetime decrease is a linear function of shock pressure in the 1-10 GPa range. So this R6G in PMMA system can be used as a PSP to monitor shock pressure at a particular location with a time resolution roughly equal to the 3 ns radiative lifetime.[51]

6. Shocks in biological systems

We have only begun to explore biological systems. Our pilot experiments used proteins with a visible chromophore dissolved in water (pH = 7 phosphate buffer). Our first experiment was performed at the Institute for Shock Physics at Washington State University, directed by Prof. Yoghendra (Yogi) Gupta, and it used horse heart met-Myoglobin, a 17 kDa protein with a heme cofactor that absorbs strongly around 400 nm.[21] The protein aqueous solution was placed in a cell between two windows which were shocked by similar window launched by a gas gun. This produces a reverberating "ring-up" shock[52] that brings the water to its final pressure in multiple stages, so it heats the water less than the single-stage prediction shown in Fig. 2. A continuous arc lamp and a streak camera were used to measure the time-dependent visible spectrum. Under static high pressure, Myoglobin denatures at about 0.8 GPa[53, 54] and we far exceeded that with a 5 GPa shock.

Pressure denaturation is known to produce a large change in the heme absorption[54] that was not observed in Fig. 9a. Instead, the most prominent feature of Fig. 9a is a large increase in the baseline over several μs. Later, Gupta's group showed that this baseline increase was due to shock freezing of water into the IceVII phase.[35] The shock creates supercooled water and the baseline increase is caused by light scattering from the ice particles as they grow. The transformation from liquid water to ice apparently inhibits Myoglobin denaturation.

In our lab we are able to reach 5 GPa pressures in a single-stage shock where water does not freeze. We used the mCherry protein, a 27 kDa protein with a strong visible emission. The chromophore is a complex of two amino acids bonded to different protein chains,[55, 56] and pressure changes of the protein structure vary the forces on these amino acids, which strongly affects the fluorescence intensity.[56] In static compression experiments, the fluorescence has

mostly disappeared by 1.5 GPa.[56] Figure 9b shows with a 5 GPa shock the emission splits into two peaks which do not decay on the experimental time scale, and which presumably represent two higher-energy conformational substates. Shock experiments can reveal the large-amplitude chain dynamics of proteins.

7. Recovery experiments

A shock recovery experiment is one where whatever remains of the target is recovered for *post mortem* analysis. For example, shocked materials might undergo a transition to a metastable phase whose structure can be measured later. Or nanodiamonds or other novel forms of carbon can be recovered from the remains of detonating a carbon-rich explosive.[57, 58]

We have studied metal-organic framework (MOF) materials under shock compression[59, 60] with the intent of developing better materials to protect equipment and personnel from damaging shocks. Shock protection materials typically have high dynamic shear strength that resist projectile penetration. Alternatively, they can be materials such as sand that dissipate or absorb shock energy. Recently, there has been interest in developing multifunctional shock protection materials that combine multiple modalities to attenuate shocks. MOFs are particularly interesting in this regard since they can be produced in the form of powders with a high density of nanopores, and unlike sand, the nanopore collapse can endothermically break strong molecular bonds.

One material we have studied is the MOF denoted ZIF-8 whose structure is depicted in Fig. 10a.[59] ZIF-8 consists of cubic unit cells with Zn atoms at the vertices and imidazole linkers. ZIF-8 is a MOF that retains its structure when desolvated, and the cubic crystals are stable with up to 50% free volume. Nanopore collapse could, theoretically, break multiple chemical bonds such as the Zn-imidazole bonds.

In our experiments, ZIF-8 powders were stabilized with a few percent polymer binder and spread on a glass plate. After flyer impact that crushes a column of ZIF-8, the flyer plate with shocked ZIF-8 can be lifted off the glass for *post mortem* analysis. Figure 10b shows a cross-section of a column of ZIF-8 before and after a 0.6 km/s impact lasting about 8 ns.[59] The shock compressed the column to about one-half its original height. The flyer plate impact was at the top of the column. Since the shock was strongly attenuated as it passed down the column, the effects of different pressures can be studied by looking at shocked material at different depths.

The image in Fig. 10b shows three different zones in the shocked ZIF-8, indicating shock attenuation proceeds by multiple mechanisms. The Raman spectrum before shock and in the three different zones is shown in Fig. 10c. At the bottom of the column where the shock was the weakest, the Raman spectrum was unaffected by shock but the cubic crystals were damaged. In the middle zone there is one big effect. The ~200 cm^{-1} transition assigned to Zn-imidazole stretch has greatly diminished in amplitude, indicating that nanopore collapse was accompanied by endothermic breaking of the Zn-imidazole bond, while the rest of the MOF structure was largely unaffected. In the top zone adjacent to the flyer plate no molecular transitions were observed, indicating an amorphous material with most of the original chemical bonds broken.[59]

These recovery experiments show that ZIF-8 is a multifunctional shock attenuator that exhibits three distinct modalities. ZIF-8 is also lightweight, and we previously showed that on a per-mass basis it attenuated shocks a factor of seven better than Plexiglas used to make bulletproof shields.[60]

8. Detonation on a tabletop

The destructive power of energetic materials (EM) is maximized by creating a detonation, first observed by Alfred Nobel. In a detonation, the energy is released in the form of

a shock wave that is sustained by chemical energy release. A detonation involves a delicate balance that causes the shock to maintain a steady profile until the EM is exhausted and its stored energy released.

To better understand detonations, researchers study the dynamics of the shock-to-detonation transition, typically using input shocks longer in duration than the exothermic stages of the complex chemistries. For detonation on a tabletop,[41, 61, 62] we design shocks to minimize the detonation build up time. That lets us use the smallest possible charges and time resolve some of the exothermic processes.

A detonation in a liquid consists of a steep rise leading to a high-pressure state called the von Neumann spike, and a trailing decay to a critical plane called the Chapman-Jouguet plane.[63] Because of the shock velocity, any process behind the Chapman-Jouguet plane cannot affect the detonation itself. The region between the spike and plane is called the reaction zone. The minimum time needed to produce a detonation is the time for the reaction zone to develop from the initiating shock. To minimize this time, we use a short-duration shock whose pressure is a bit larger than the von Neumann spike, so it mimics the front end of the detonation, and it does not have to evolve very much to create a reaction zone.[41]

These experiments were done on liquid nitromethane (NM), CH_3NO_2, a model system for homogeneous explosives, which decomposes into a mixture of CO, CO_2, H_2O, N_2 and various carbon or nitrogen-doped carbon species (soot),[64] while releasing 5 kJ/cm^3 at about 3500K and 13 GPa pressure in the Chapman-Jouguet plane.[65]

Figure 11 shows how a shock evolves in NM from a 4 km/s impact lasting 4 ns, producing an input pressure of 18 GPa, compared to the steady detonation pressure of 13 GPa and the reaction zone of 11 ns or 70 μm in length.[41] The experiment was done by fabricating

disposable arrays of liquid cuvettes[66] having different thicknesses. For each thickness, PDV was used to measure the profile of the shock exiting the NM. Figure 11 shows that after a delay of several nanoseconds a thermal explosion occurs, causing the shock pressure to rise to about 35 GPa. After this decay, around 10 ns, the waveforms propagate without changing their profile, so we have produced a chemically-sustained shock that maintains a constant profile: a detonation. The detonation was produced in 50 μg of NM, so unlike studying bombs, this is a process that can be performed safely on a tabletop.

Besides these velocity and pressure measurements, we could complete the study using our optical pyrometer to determine the temperature,[41] as shown in Fig. 12a. This is done by measuring the time-dependent spectral radiance of the thermal emission. The spectral radiance is the absolute intensity of the emission spectrum ($W/sr/m^2/nm$) measured against a calibrated standard. The spectral radiance can be converted into a temperature by fitting it to Planck's blackbody distribution. Since NM is not black, we have to use a modified form called the graybody, which has the same spectral distribution but a lower intensity than a blackbody. Figure 12a shows spectral radiances obtained at two different times along with the corresponding graybody fits.[41]

With such a small sample the detonation lasts only a short time, so it produces thermal emission for only 25 ns (Fig. 12b). During the detonation the temperature has a steady value of 3430 ± 240K.[41]

9. Catalysis in a shock

Catalysts increase reaction rates by lowering energetic barriers without changing the products. In shock chemistry, such as the NM detonation discussed above, a catalyst may also

have a big effect on the reactive flow, so catalysts in shock chemistry have the potential to affect chemistry in two distinct ways.

Amines are well known to catalyze NM shock ignition. The usual view of amine sensitization treats the amine as a catalyst that lowers the barrier to ignition,[67] which might also lower the shock pressure needed to produce detonation. Theoretical calculations using density-functional theory molecular dynamics[68-70] or ReaxFF molecular dynamics[68, 70] show that the first step in NM shock ignition is proton transfer that produces CH_2NO_2H from CH_3NO_2. NM is a weak acid that becomes much stronger at high temperatures and pressures. Proton transfer leads to a series of reactions rate-limited by breaking the C-N bond, culminating in the first highly-exothermic step, production of H_2O.[64]

We studied NM with 1% added ethylenediamine catalyst (NM/EDA).[62] In Fig. 13a, we plot the energy difference between the (time-integrated) outgoing and incoming shocks in NM and NM/EDA, in units of the shock energy fluence (kJ/m^2), versus the imparted fluid velocity U_p. At low velocities there is minimal shock attenuation. As the impact velocity is increased, there is a critical velocity where NM becomes absorbing. With velocities just above the absorption maximum there is a large increase in the output shock energy. This large increase is driven by NM ignition, as observed by a sudden increase in thermal emission. Figure 13a shows that the EDA catalyst lowers the velocity needed to trigger both shock absorption and energy release.[62]

Figure 13b shows the Hugoniot equations of state, a plot of shock velocity versus fluid velocity. Our NM Hugoniot is identical to what was observed by numerous workers in this field.[41] But the NM/EDA Hugoniot is quite different at lower velocities. At the same fluid velocity, the shock velocity in NM/EDA is significantly slower, at some speeds by almost a

factor of two. When the fluid is flowing at the same rate but the shock is slower, the shocked fluid is denser and hotter. Using the well-known relation $\rho_s = \rho_0/(1-U_p/U_s)$,[22] we can show that at times the shock density ρ_s of NM/EDA is 30% greater than in NM.[62] Higher compressibility is associated with greater adiabatic heating, so EDA both lowers the barrier to proton transfer reactions and increases shock energy conversion into heat. To explain this enhanced compressibility, we proposed that shocked NM/EDA has so much proton transfer that it produces a reactive flow with a much higher ionic strength than in NM. The sudden transformation from a molecular liquid to an ionic liquid with stronger intermolecular interactions is responsible for enhanced compressibility and shock heating.[62] Thus, the catalyst lowers the threshold for shock ignition in two ways, the usual barrier lowering plus a physical transformation that enhances the amount of shock energy absorbed by the fluid.

10. Shocked interfaces

Our ability to probe molecules at interfaces has improved dramatically with the development of femtosecond vibrational sum-frequency generation (SFG).[71] SFG is sensitive, despite the small number of interfacial molecules, because the output signal is a coherent pulse. SFG is interface selective, minimizing signals from the vastly greater centrosymmetric bulk because SFG vanishes in centrosymmetric media. Using the broadband nature of femtosecond pulses, it becomes possible to obtain an entire SFG spectra on a single shot,[72, 73] so this technique makes it possible to probe interfacial molecules during shock compression.[74, 75]

One reason to study shocked interfaces is to understand the behavior of interfacial molecules under extreme conditions, for instance a lubricant adjacent to a moving metal part. The other reason is to achieve high time resolution by probing the shock as it moves across a monolayer.

For our experiments, we chose a model system, the self-assembled monolayer (SAM) consisting of octadecylthiol (ODT) on Au. ODT is a 2 nm thick crystalline layer of all-*trans* hydrocarbon chains anchored to the Au surface through a thiolate linkage,[76] as illustrated in Fig. 14. In fact, SFG selectively probes only the terminal methyl groups of the chains, a layer only 1.5Å thick,[77] since the rest of the chains are nominally centrosymmetric. Using mid-IR femtosecond pulses, it is possible to see two CH-stretching transitions of the methyl groups, and from the intensity ratio for these symmetric and antisymmetric stretches it is possible to measure the time-dependent tilt angle of the methyl group relative to surface normal (Fig. 14b).[11, 74]

The sample configuration for these experiments is depicted in Fig. 14a. For this high time resolution experiment we generated the shock by femtosecond confined ablation of the Cr adhesion layer below the Au surface.[11] To protect Au and the SAM from hot electrons generated in the ablation, we used a Ni insulation layer, since Ni has efficient electron damping by phonons. The shock passes over the SAM into an impedance-matched fluid. Since SFG probing of CH-stretch transitions is around 3.3 μm in the IR, the fluid was deuterated and the window was CaF_2.[11]

Figure 15 shows the time-dependent intensities of the symmetric and anti-symmetric CH stretching transitions at different laser pulse energies that produced shocks up to about 2 GPa. In Fig. 15a, the shock, with a rise time <4 ps, causes both transitions to lose intensity and then recover. The intensity loss is caused by the shock bending the SAM terminal methyl groups to larger tilt angles. At the highest shock pressure (Fig. 15d) the methyl tilt does not recover. A series of simulations we did showed that this irreversible tilt resulted from a *trans*-to-*gauche* conversion of the alkane bonds just beneath the terminal methyl groups.[78]

11. Summary

We have developed a reliable high-throughput tabletop hypersonic flyer plate launcher that uses a single-box Q-switched Nd:YAG laser that, along with a velocimeter such as a photon Doppler velocimeter (PDV) and an inverted microscope, forms the core of the shock compression microscope. The other element needed for high-throughput studies is the ability to mass-produce arrays of single-use samples, and here we have described several ways to do this. Since laser microscope experiments have become standard in many laboratories, many methods already exist to probe samples. I have provided a brief introduction to shock waves in solids and liquids, and then described several ways we have used this technology to study molecular phenomena of interest to physical chemistry or chemical physics researchers.

12. Perspective

With a tabletop flyer plate launcher, researchers can create extreme conditions, albeit ones that persist only briefly, in virtually any liquid or solid, with the push of a button. It is an intrinsically safe method even for studying high explosives, although please keep your eyes out of the laser beam and your fingers away from the flyer plates.

The shock microscope can be contrasted with another method to produce high temperatures and pressures, a heated or laser-heated diamond anvil cell (DAC). Using a DAC is not a high-throughput technique. It takes a long time to load the cell without breaking the diamonds, and a long time to bring it to high temperature. For the molecular materials discussed here, by the time the DAC is brought to temperature the sample will have decomposed. Another convenient and complementary tabletop method for hypervelocity impacts, laser microparticle launching, is not discussed here except to note it has been thoroughly reviewed recently[79] and shooting microparticles at samples is quite different from launching powerful planar shock waves.

The experiments reported here were done with a single-box multiamplifier Nd:YAG laser that produces 2.5J pulses, but previously we have described how to launch flyers with the widely available single-head 0.8J Nd:YAG laser,[15] albeit with a lower velocity ceiling of about 1.6 km/s, so these techniques can be easily adopted by researchers using equipment common in laser laboratories.

The intent of this perspective is to illustrate the wide range of possibilities for future research in this area, and to demonstrate that the barrier to entering this field is not very high. Here we described studies of molecular photophysics under extreme conditions, the use of photoemissive probes to study shocks in inhomogeneous materials, dynamics of proteins in aqueous buffer, engineered molecular frameworks (MOFs), the ease of recovering samples for leisurely *post-mortem* studies, the ability to produce and study powerful detonations on a tabletop, the intriguing behavior of chemical catalysis in a shocked material, and the use of nonlinear coherent spectroscopy to study shocked interfaces with Angstrom spatial resolution.

Going forward, there are a few future possibilities I would like to illustrate. One is the chemistry of extreme water and its interactions with solutes, which has hardly been studied due to the difficulties in producing extreme water. Extreme water is the best candidate for the so-called "universal solvent" since it would surely oxidize most container materials. Since water is ubiquitous in biology, shocking biological systems allows researchers to study structural relaxation not in the usual linear response regime, but with sudden large-amplitude perturbations. There are notable medical applications that use shock waves, among them kidney stone fragmentation and ocular cornea ablation, but the molecular consequences of applying shock waves to biological systems are hardly understood. Imagine what might happen to a biological

system after the biological water [80] is suddenly--but briefly--converted from a hydrogen-bonded liquid to a molten salt.

The dynamics of phase transitions is another interesting field which is dominated by experiments studying solid-to-liquid (i.e. melting) transitions, since it is easy to melt a solid with a laser pulse. The reverse process, solidification or crystallization, is more difficult since it involves rapidly creating order out of disorder. Because water is one of the few substances where the liquid state volume exceeds the solid volume, shocking water produces supercooled water that rapidly crystallizes. In the shock experiments described here, water crystallization was observed via light scattering, which measures the rate of formation of water crystals large enough to scatter light, say 100 nm or more. These larger crystals originate as tiny molecular nucleation sites which cannot be "seen" but whose properties can be studied with time-resolved molecular spectroscopy.

Another emerging opportunity for chemists involves hypervelocity missiles, spacecraft and cometary or meteoric impacts. Our flyer plates are tiny hypersonic vehicles that can fly through atmosphere or vacuum or can mimic cometary impacts. Hypersonic missiles exceed Mach 5 (1.5 km/s) as they travel through the atmosphere. A lot of chemistry occurs when the missile strikes atmospheric water droplets or dust (mainly silica) which degrades the missile surface, especially the sensor windows. Spacecraft materials degrade by hypersonic impacts with micrometeorites. A big problem is developing materials to withstand such harsh conditions, so high-throughput tabletop measurements should prove useful for damage characterization and elucidation of fundamental mechanisms. Cometary impacts can produce metastable phases of materials, and impacts with small molecules such as ammonia, carbon dioxide and water present

in the early Earth can synthesize prebiotic molecules such as amino acids needed for life to develop.[81, 82]

Our experiments using nonlinear coherent vibrational spectroscopy to probe molecules at interfaces suggest that the application of such techniques in shock waves could be a useful way to study molecular relaxation following sudden large-amplitude perturbations or to better understand molecular lubrication at rapidly moving interfaces.

Now we have the ability to turn laser pulses into bullets. It is a whole new world for laser spectroscopy.

Conflicts of interest

There are no conflicts to declare.

Acknowledgements

The research described in this study is based on work at the University of Illinois, currently supported by the US Air Force Office of Scientific Research under awards FA9550-19-1-0027 and FA9550-19-1-0318, and the US Army Research Office under awards W911NF-19-2-0037 and W911NF-16-1-0406.

References

1. D. D. Dlott, in *Laser Spectroscopy of Solids II*, ed. W. Yen, Springer Verlag, Berlin1988, pp. 167-200.
2. J. C. Deàk, L. K. Iwaki, S. T. Rhea and D. D. Dlott, *J. Raman Spectrosc.*, 2000, **31**, 263-274.
3. R. D. Bardo, *Int. J. Quantum Chem.: Quantum Chem. Symp.*, 1986, **20**, 455-469.
4. C. S. Coffey and E. T. Toton, *J. Chem. Phys.*, 1982, **76**, 949-954.
5. D. D. Dlott, in *Overviews of recent research on energetic materials*, eds. D. Thompson, T. Brill and R. Shaw, World Scientific, Hackensack, New Jersey2005, pp. 303-333.
6. D. D. Dlott and M. D. Fayer, *J. Chem. Phys.*, 1990, **92**, 3798-3812.
7. A. Tokmakoff, M. D. Fayer and D. D. Dlott, *J. Phys. Chem.*, 1993, **97**, 1901-1913.
8. M. R. Armstrong, T. C. Germann and J. M. D. Lane, eds., *Shock Compression of Condensed Matter 2019*, AIP Publishing2019.
9. J. W. Forbes, *Shock Wave Compression of Condensed Matter. A Primer*, Springer, New York, 2012.
10. M. S. Powell, P. R. Bowlan, S. F. Son, C. A. Bolme, K. E. Brown, D. S. Moore and S. D. McGrane, *Rev. Sci. Instrumen.*, 2019, **90**.
11. J. E. Patterson, A. S. Lagutchev, W. Huang and D. D. Dlott, *Phys. Rev. Lett.*, 2005, **94**, 015501.
12. D. D. Dlott, S. Hambir and J. Franken, *J. Phys. Chem. B*, 1998, **102**, 2121-2130.
13. W. P. Bassett, B. P. Johnson, L. Salvati, E. J. Nissen, M. Bhowmick and D. D. Dlott, *Propell. Explos. Pyrotech.*, 2020, **45**, 222-235.

14. D. D. Dlott, M. Akhtar, W. P. Bassett, M. Bhowmick, B. P. Johnson, S. M. Matveev, E. J. Nissen, L. Salvati III, S. Stekovic, W. Zhang and X. Zhou, *AIP Conf. Proc.*, 2020, **2272**, 060009

15. K. E. Brown, W. L. Shaw, X. Zheng and D. D. Dlott, *Rev. Sci. Instrum.*, 2012, **83**, 103901.

16. A. D. Curtis, A. A. Banishev, W. L. Shaw and D. D. Dlott, *Rev. Sci. Instrum.*, 2014, **85**, 043908.

17. A. A. Banishev, W. L. Shaw, W. P. Bassett and D. D. Dlott, *J. Dyn. Behav. Mater.*, 2016, **2**, 194-206.

18. S. A. Hambir, J. Franken, D. E. Hare, E. L. Chronister, B. J. Baer and D. D. Dlott, *J. Appl. Phys.*, 1997, **81**, 2157-2166.

19. G. Tas, J. Franken, S. A. Hambir and D. D. Dlott, *Phys. Rev. Lett.*, 1997, **78**, 4585-4588.

20. M. Bhowmick, W. P. Bassett, S. M. Matveev, L. Salvati III and D. D. Dlott, *AIP Adv.*, 2018, **8**, 125123.

21. D. D. Dlott, *Annu. Rev. Phys. Chem.*, 2011, **62**, 575-597.

22. S. P. Marsh, *LASL Shock Hugoniot Data*, University of California Press, Berkeley, CA, 1980.

23. Y. B. Zel'dovich and Y. P. Raiser, *Physics of Shock Waves and High-temperature Hydrodynamic Phenomena*, Academic Press, New York, 1966.

24. J. W. Swegle and D. E. Grady, *J. Appl. Phys.*, 1985, **58**, 692-701.

25. P. J. S. van Capel and J. I. Kijkhuis, *Appl. Phys. Lett.*, 2006, **88**, 151910.

26. C. A. Bolme, S. D. McGrane, D. S. Moore and D. J. Funk, *J. Appl. Phys.*, 2007, **102**, 033513

27. V. H. Whitley, S. D. McGrane, D. E. Eakins, C. A. Bolme, D. S. Moore and J. F. Bingert, *J. Appl. Phys*, 2011, **109**, 013505

28. A. C. Mitchell and W. J. Nellis, *J. Chem. Phys.*, 1982, **76**, 6273-6281.

29. J. M. Walsh and M. H. Rice, *J. Chem. Phys.*, 1957, **26**, 815-823.

30. G. A. Lyzenga, T. J. Ahrens, W. J. Nellis and A. C. Mitchell, *J. Chem. Phys*, 1982, **76**, 6282-6286.

31. W. B. Holzapfel, *J. Chem. Phys.*, 1969, **50**, 4424-4428.

32. S. Ridah, *J. Appl. Phys.*, 1988, **64**, 152-158.

33. A. E. Gleason, C. A. Bolme, E. Galtier, H. J. Lee, E. Granados, D. H. Dolan, C. T. Seagle, T. Ao, S. Ali, A. Lazicki, D. Swift, P. Celliers and W. L. Mao, *Physical Review Letters*, 2017, **119**.

34. E. J. Nissen and D. H. Dolan, *J. Appl. Phys.*, 2019, **126**, 015903.

35. D. H. Dolan, J. N. Johnson and Y. M. Gupta, *J. Chem. Phys.*, 2005, **123**, 064702-064710.

36. N. Goldman, E. J. Reed, I.-F. W. Kuo, L. E. Fried, C. J. Mundy and A. Curioni, *J. Chem. Phys.*, 2009, **130**, 124517.

37. E. Schwegler, G. Galli, F. Gygi and R. Q. Hood, *Phys Rev. Lett.*, 2001, **87**, 265501.

38. O. T. Strand, D. R. Goosman, C. Martinez, T. L. Whitworth and W. W. Kuhlow, *Rev. Sci. Instrum.*, 2006, **77**, 083108.

39. J. Weng, X. X. Wang, Y. Ma, H. Tan, L. Cai, J. Li and C. Liu, *Rev. Sci. Instrum.*, 2008, **79**, 113101.

40. W. P. Bassett, B. P. Johnson and D. D. Dlott, *Propell. Explos. Pyrotech.*, 2020, **45**, 338-346.

41. M. Bhowmick, E. J. Nissen and D. D. Dlott, *J. Appl. Phys.*, 2018, **124**, 075901.

42. W. P. Bassett and D. D. Dlott, *Rev. Sci. Instrum.*, 2016, **87**, 103107.

43. A. A. Banishev, J. M. Christensen and D. D. Dlott, *AIP Confer. Proc.*, 2017, **1793**, 060010.

44. J. W. Gregory, K. Asai, M. Kameda, T. Liu and J. P. Sullivan, *Proceedings of the Institution of Mechanical Engineers, Part G: Journal of Aerospace Engineering*, 2008, **222**, 249-290.

45. J. I. Peterson and R. V. Fitzgerald, *Rev. Sci. Instrum.*, 1980, **51**, 670-671.

46. J. H. Bell, E. T. Schairer, L. A. Hand and R. D. Mehta, *Annu. Rev. Fluid Mech.*, 2001, **33**, 155-206.

47. A. A. Banishev and D. D. Dlott, *J. Appl. Phys.*, 2014, **115**, 203515.

48. A. A. Banishev, W. L. Shaw and D. D. Dlott, *Appl. Phys. Lett.*, 2014, **104**, 101914.

49. H. G. Drickamer, *Annu. Rev. Phys. Chem.*, 1982, **33**, 25-47.

50. P. I. H. Bastiaens and A. Squire, *Trends in Cell Biology*, 1999, **9**, 48-52.

51. W.-L. Liu, W. P. Bassett, J. M. Christensen and D. D. Dlott, *J. Phys. Chem. A*, 2015, **119**, 10910–10916.

52. G. T. Sutherland, Y. M. Gupta and P. M. Bellamy, *J. Appl. Phys.*, 1986, **59**, 1141-1146.

53. W. Doster and R. Gebhardt, *Chem. Phys.*, 2003, **292**, 383-387.

54. A. Zipp and W. Kauzmann, *Biochem.*, 1973, **12**, 4217-4228.

55. D. von Stetten, M. Noirclerc-Savoye, J. Goedhart, T. W. J. Gadella and A. Royant, *Acta Crystallographica Section F: Structural Biology and Crystallization Communications*, 2012, **68**, 878-882.

56. E. A. Pozzi, L. R. Schwall, R. Jimenez and J. M. Weber, *J. Phys. Chem. B.*, 2012, **116**, 10311-10316.

57. S. Bastea, *Scientific Reports*, 2017, **7**, 42151.

58. Y. P. Zhang, Z. Yang, Q. K. Li and Y. H. He, *Acta Chim. Sin.*, 2018, **76**, 556-563.

59. X. Zhou, Y. Miao, K. S. Suslick and D. D. Dlott, *Acct. Chem. Res.*, 2020, **53**, 2806-2815.

60. X. Zhou, Y.-R. Miao, W. L. Shaw, K. S. Suslick and D. D. Dlott, *J. Am. Chem. Soc.*, 2019, **141**, 2220-2223.

61. E. J. Nissen, M. Bhowmick and D. D. Dlott, *Combust. Flame*, 2021, **225**, 5-12.

62. E. J. Nissen, M. Bhowmick and D. D. Dlott, *J. Phys. Chem. B.*, 2021, **125**, 8185-8192.

63. C. M. Tarver and P. A. Urtiew, *J. Energ. Mater.*, 2010, **28**, 299-317.

64. S. P. Han, A. C. T. van Duin, W. A. Goddard and A. Strachan, *J. Phys. Chem. B*, 2011, **115**, 6534-6540.

65. R. Meyer, J. Köhler and A. Homberg, *Explosives, seventh edition*, Wiley VCH, New York, 2016.

66. E. J. Nissen, M. Bhowmick and D. D. Dlott, *AIP Conf. Proc.*, 2020, **2272**, 030024

67. Y. A. Gruzdkov and Y. M. Gupta, *J. Phys. Chem. A*, 1998, **102**, 2322-2331.

68. M. R. Manaa, E. J. Reed, L. E. Fried, G. Galli and F. Gygi, *J. Chem. Phys.*, 2004, **120**, 10146–10153.

69. P. Politzer, J. M. Seminario and A. G. Zacarias, *Mol. Phys.*, 1996, **89**, 1511-1520.

70. R. Perriot, M. J. Cawkwell, E. Martinez and S. D. McGrane, *J. Phys. Chem. A*, 2020, **124**, 3314-3328.

71. P. Guyot-Sionnest, J. H. Hunt and Y. R. Shen, *Phys. Rev. Lett.*, 1987, **59**, 1597-1600.

72. L. J. Richter, T. P. Petralli-Mallow and J. C. Stephenson, *Opt. Lett.*, 1998, **23**, 1594-1596.

73. A. Lagutchev, A. Lozano, P. Mukherjee, S. A. Hambir and D. Dlott, *Spectrochim. Acta. A*, 2010, **75**, 1289–1296.

74. A. S. Lagutchev, J. E. Patterson, W. Huang and D. D. Dlott, *J. Phys. Chem. B*, 2005, **109**, 5033-5044.

75. J. Patterson, A. S. Lagutchev and D. D. Dlott, *AIP Confer. Proc.*, 2004, **706**, 1299-1302.

76. D. L. Alara and R. G. Nuzzo, *Langmuir*, 1985, **1**, 52-66.

77. A. L. Harris, C. E. D. Chidsey, N. J. Levinos and D. N. Loiacono, *Chem. Phys. Lett.*, 1987, **141**, 350-356.

78. J. E. Patterson and D. D. Dlott, *J. Phys. Chem. B*, 2005, **109**, 5045-5054.

79. D. Veysset, J.-H. Lee, M. Hassani, S. E. Kooi, E. L. Thomas and K. A. Nelson, *Appl. Phys. Rev.*, 2021, **8**, 011319.

80. B. Bagchi, *Water in Biological and Chemical Processes: From Structure and Dynamics to Function*, Cambridge University Press, Cambridge, 2013.

81. Y. Furukawa, T. Sekine, M. Oba, T. Kakegawa and H. Nakazawa, *Nat. Geosci.*, 2008, **2**, 62-66.

82. I. Barak and A. Bar-Nun, *Origins of life*, 1975, **6**, 483-506.

83. B. P. Johnson, X. Zhou, H. Ihara and D. D. Dlott, *J. Phys Chem. A*, 2020, **124**, 4646-4653.

84. D. D. Dlott, *Annu. Rev. Phys. Chem.*, 1999, **50**, 251-278.

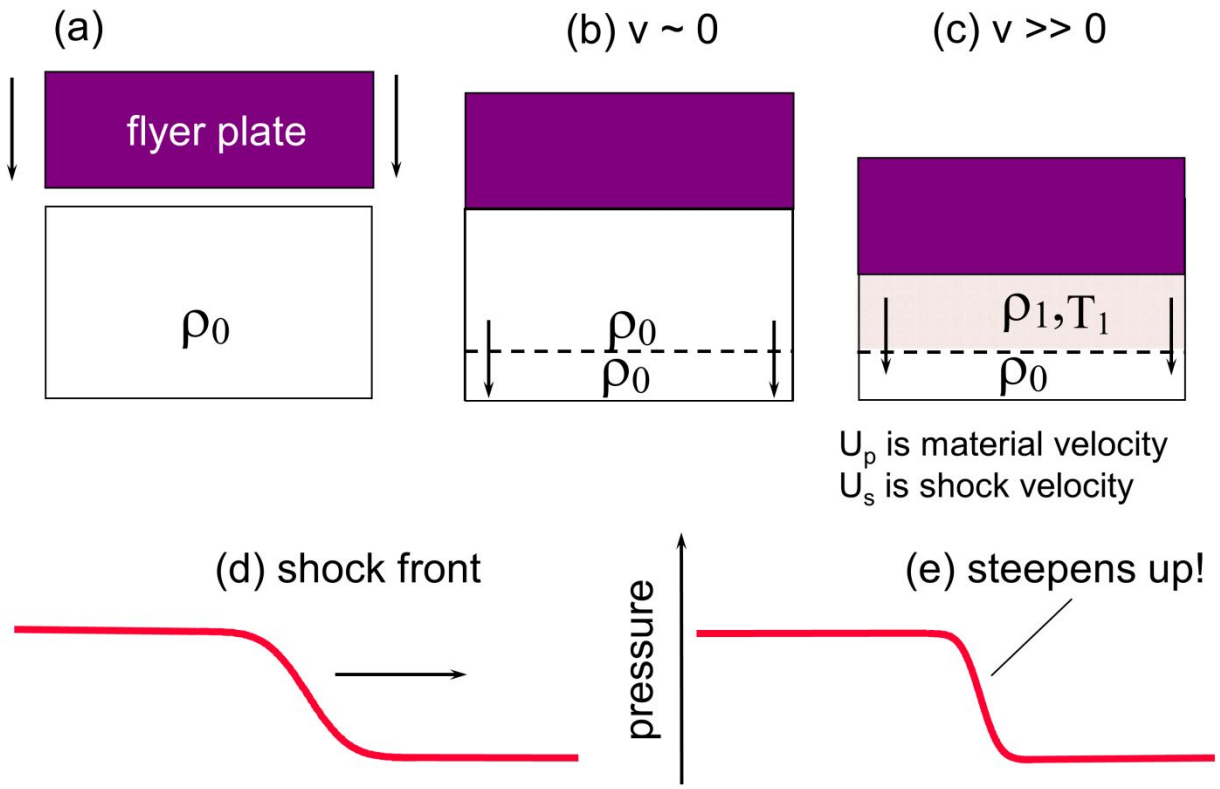

Fig. 1 What is a shock wave? (a) A disc-shaped flyer plate creates a planar impact on a material initially at density ρ_0. (b) A low-velocity $v \sim 0$ impact launches a dispersive acoustic wavepacket that produces a minimal density change. (c) A higher-velocity $v >> 0$ impact, causing the material to move at velocity U_p, launches a shock wave. Behind the shock front the material is compressed to density ρ_1 and heated to temperature T_1. (d) A shock front with a finite rise time. (e) The shock is a nonlinear excitation that can steepen as it propagates.

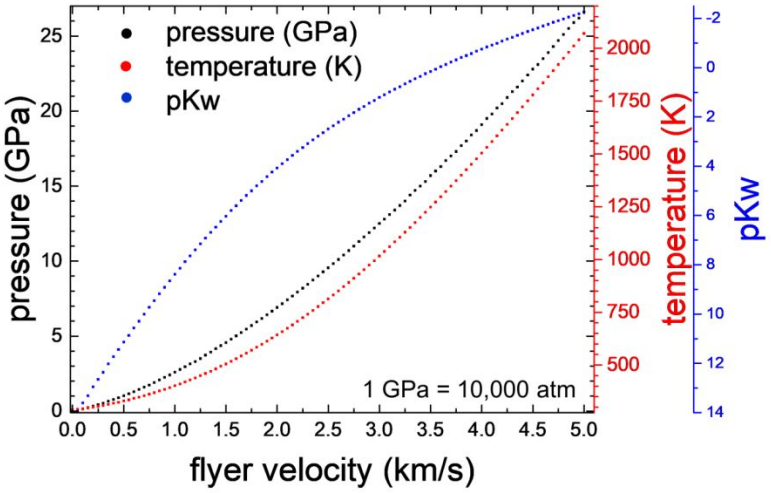

Fig. 2 Computed phase diagram for water impacted up to 5 km/s by an Al flyer plate. pKw decreases dramatically due to shock polarization, since the ion pair has a higher density than the hydrogen-bonded molecules.

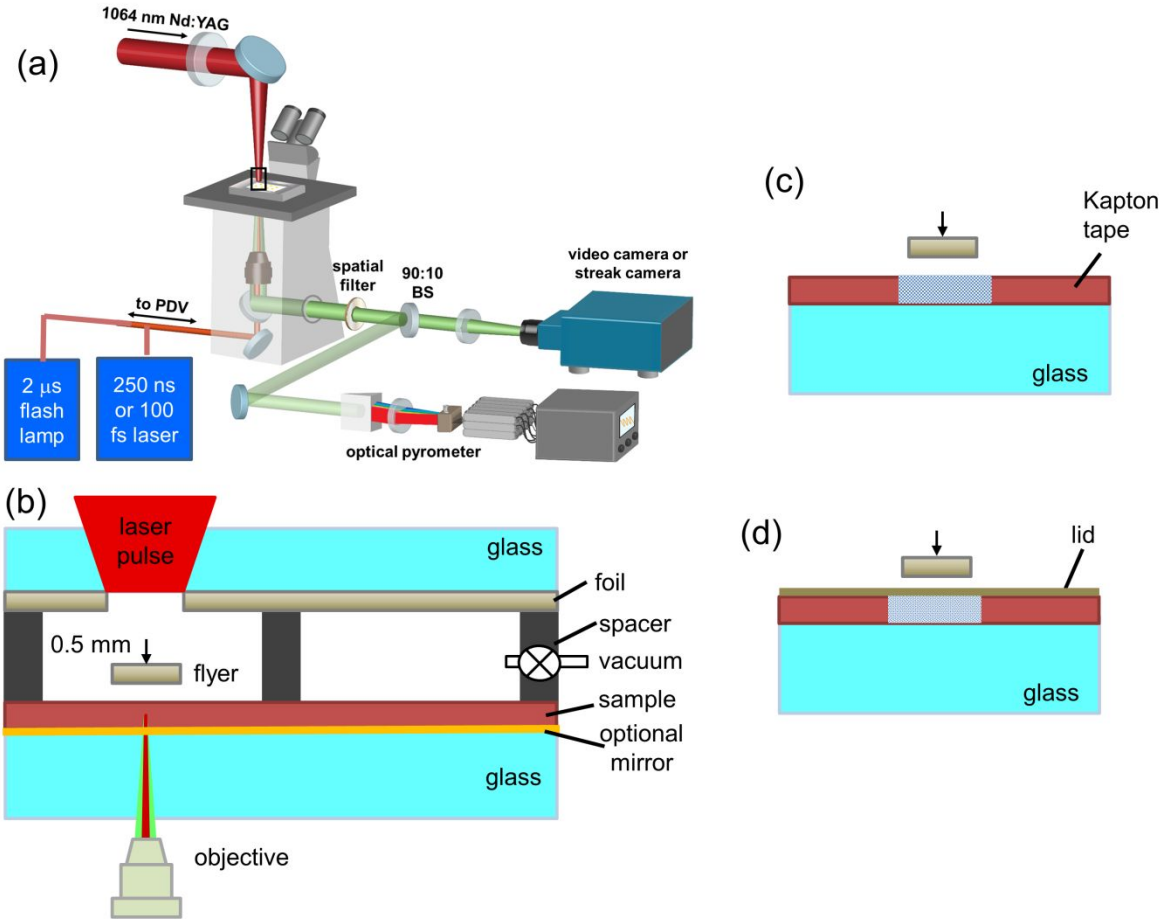

Fig. 3 (a) Schematic of a shock compression microscope with a Nd:YAG laser launcher and a photon Doppler velocimeter (PDV). The microscope in the Dlott lab has continuous and pulsed illumination sources, a nanosecond video camera, a streak camera and a high dynamic range spectrograph that can function as an optical pyrometer. BS = beamsplitter. (b) Schematic of a multitarget array (illustrating two targets) for high-throughput studies. (c) Schematic of a flyer plate impacting a solid sample observed through a glass window or "witness plate". (d) A microcuvette for liquid studies uses a thin foil lid impedance-matched to the flyer plate. Part (a) reproduced by permission from ref. [83], copyright American Chemical Society.

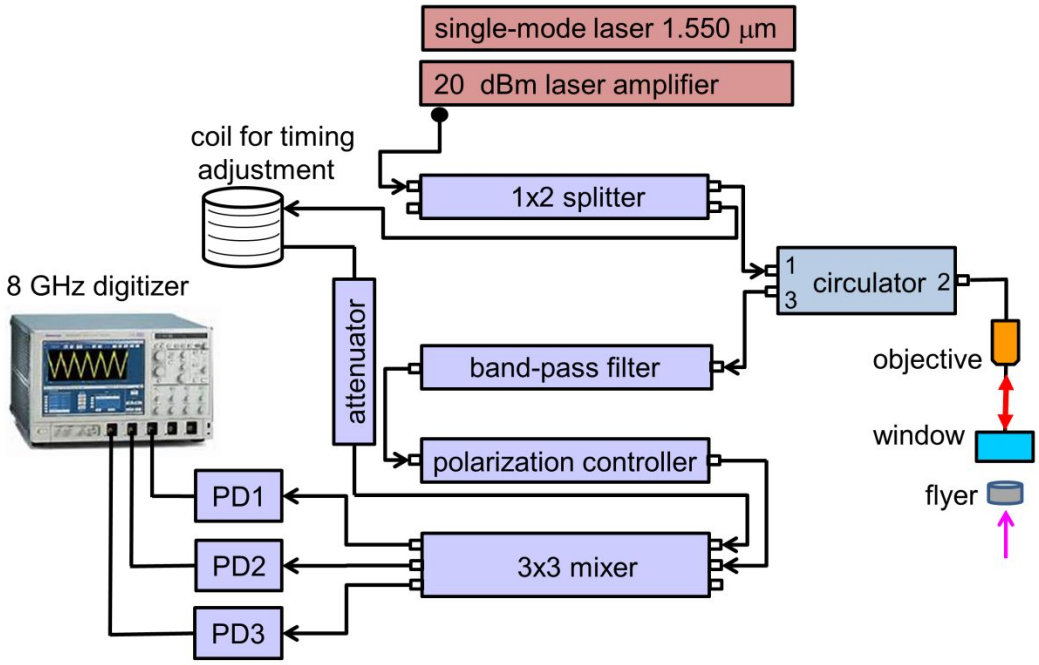

Fig. 4 Schematic of an all-fiberoptic photon Doppler velocimeter (PDV). The moving flyer plate is one mirror of an interferometer. The velocity profile of the flyer or the flyer/window interface can be extracted from the time-dependent beat profile, knowing the laser wavelength.

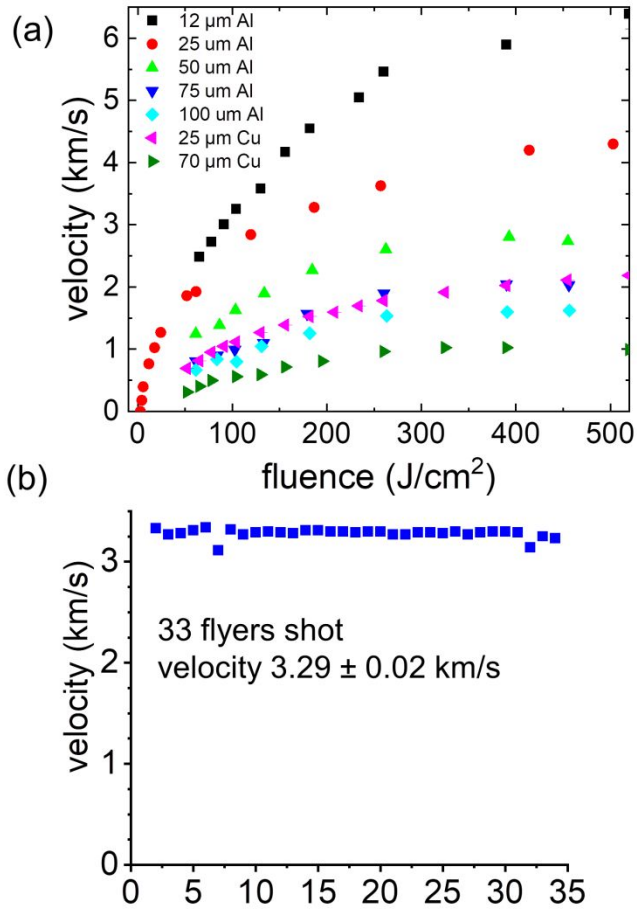

Fig. 5 (a) Flyer plate velocities as a function of launch laser fluence for different thickness Al and Cu flyers. (b) Reproducibility test on 25 μm thick Al flyer plates. Adapted with permission from ref. [17], copyright Springer Nature.

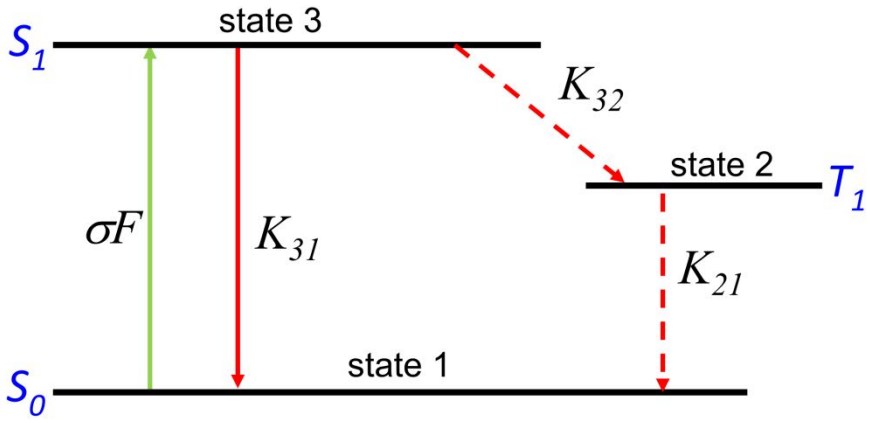

Fig. 6 A three-level Jablonsky energy level diagram for R6G dye, defining the rate constants K_{ij}. F is the input laser fluence and σ the absorption cross-section. Reproduced by permission from ref. [47], copyright American Institute of Physics.

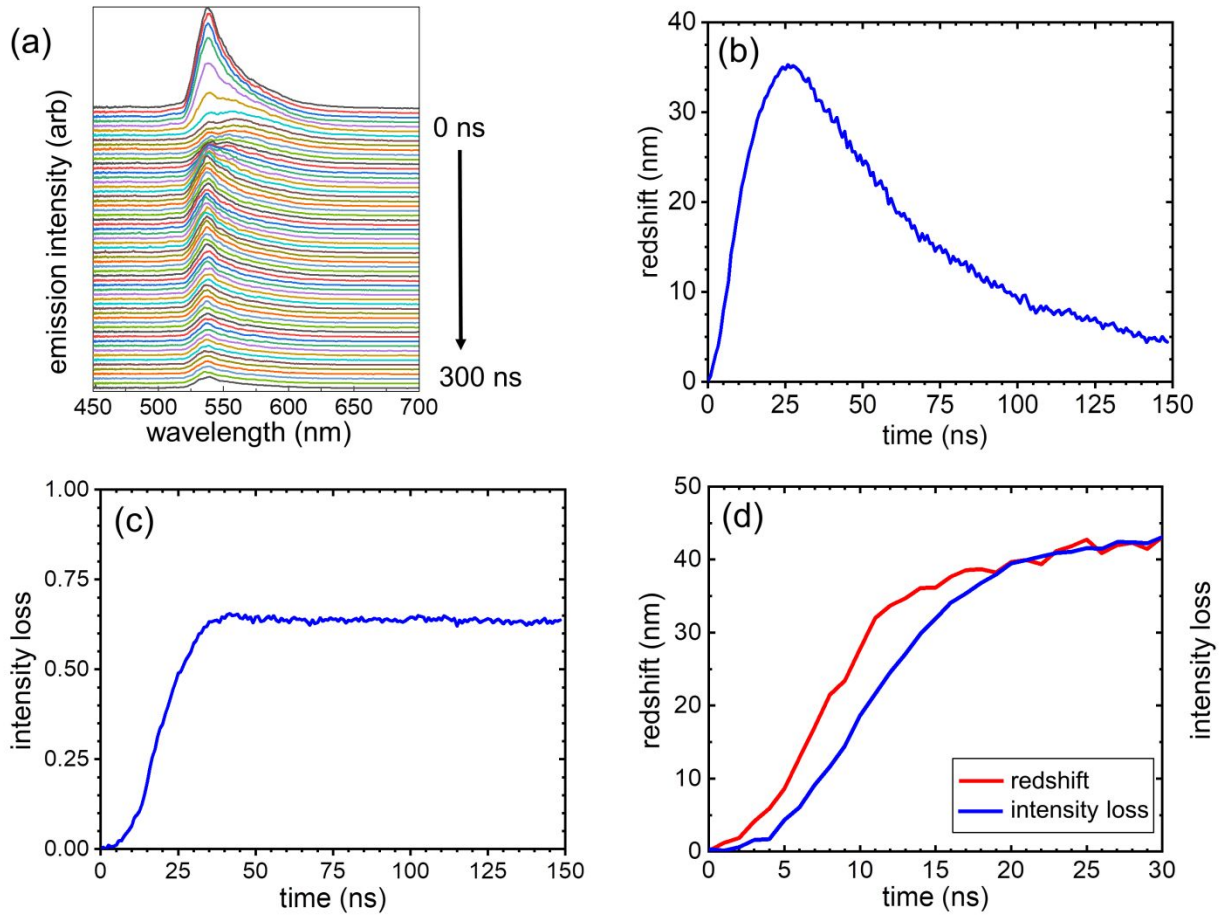

Fig. 7 (a) Fluorescence from R6G in PMMA after a 1.1 km/s impact producing a pressure of 3.9 GPa shows a temporary redshift and a persistent intensity loss. (b) Shock-induced redshift. (c) Shock-induced intensity loss. (d) The redshift appears instantaneously but the intensity loss due to intersystem crossing to dark triplet state T_1 appears after a 7 ns delay. Adapted by permission from ref. [47], copyright American Institute of Physics.

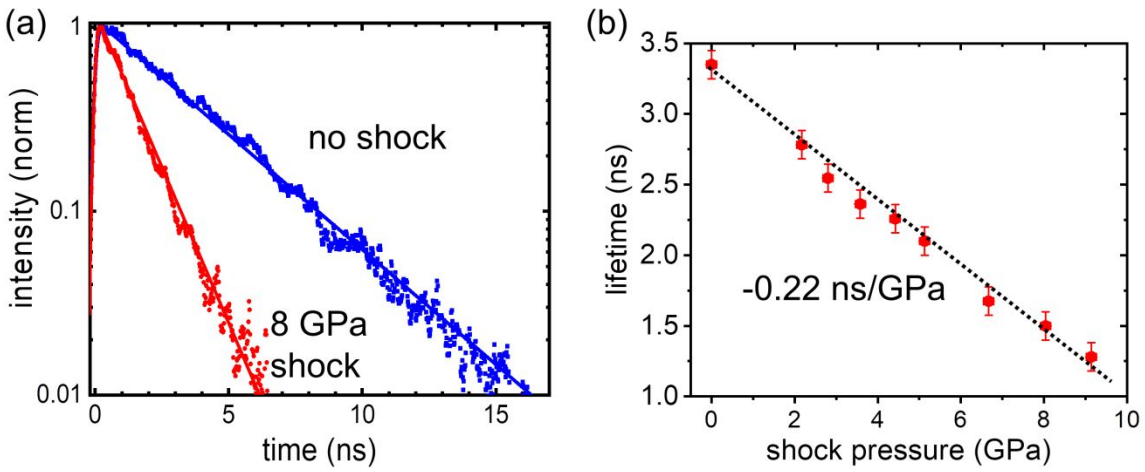

Fig. 8 R6G fluorescence lifetime in PMMA decreases during an 8 GPa shock with 18 ns duration due to enhanced nonradiative relaxation. (b) The lifetime decrease is a linear function of shock pressure so the lifetime can be used to measure shock pressure. Reproduced with permission from ref. [51], copyright American Chemical Society.

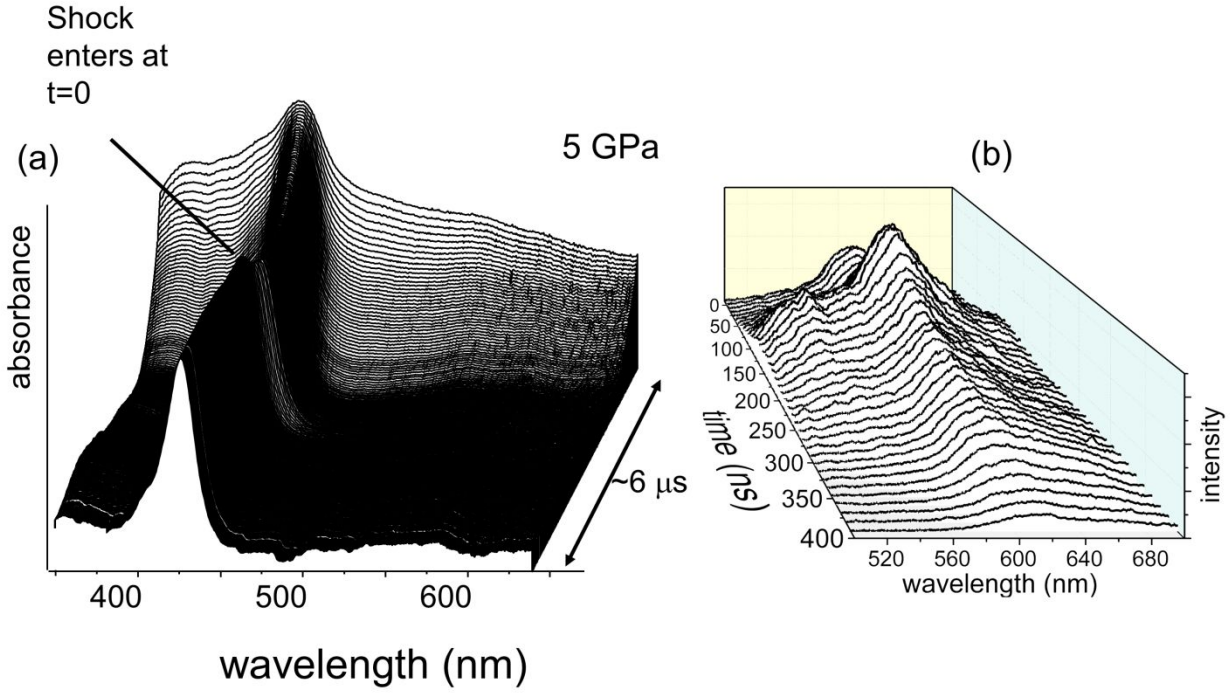

Fig. 9 (a) Absorbance spectrum of met-myoglobin protein in buffered water during a 5 GPa ring-up shock. The baseline rise is caused by the formation of IceVII crystals. (b) Emission spectrum of mCherry fluorescent protein in buffered water with a 5 GPa shock shows a structural transition that splits the electronic transition. Part (a) is reproduced with permission from ref. [84].

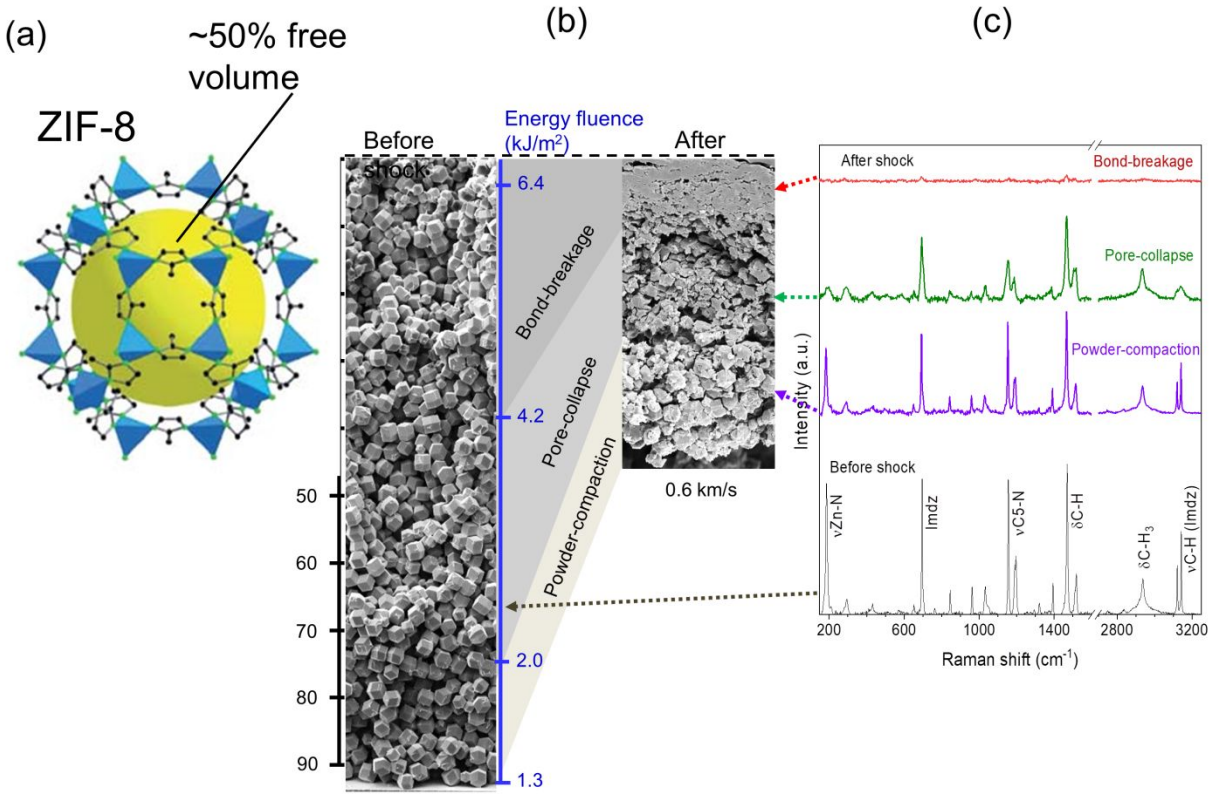

Fig. 10 (a) Structure of the metal-organic framework (MOF) denoted ZIF-8 that is about 50% nanoporous. (b) Electron micrographs of cross-sections of recovered samples of ZIF-8 crystals before and after a 0.6 km/s impact. The shock is strongly attenuated as it propagates downward. Three zones indicating three different damage mechanisms are observed. (c) The corresponding Raman spectra. In the bottom zone where the shock was weakest, the spectrum was unchanged. In the middle zone the Zn-imidazole stretch ($\nu_{Zn\text{-}N}$) transition at 200 cm^{-1} is missing, indicating broken bonds produced during pore collapse. In the top zone where the shock was strongest, the material became compact and amorphous. Reproduced with permission from ref. [60]. Copyright 2019 American Chemical Society.

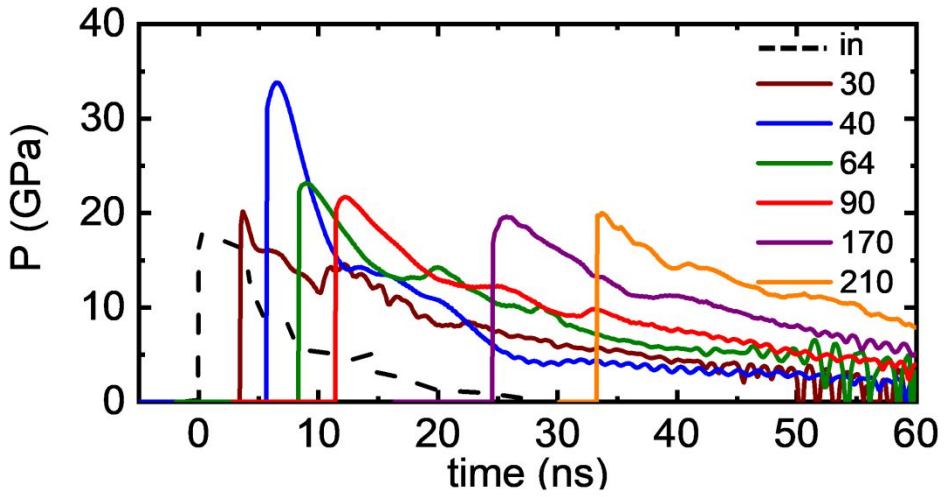

Fig. 11 An 18 GPa input shock propagating through different thickness layers (indicated at right in μm) of nitromethane (NM), measured with PDV. After a few nanoseconds there is a powerful explosion, jumping the pressure to >30 GPa. This large shock, called a "superdetonation", decays into a detonation, a shock that maintains a constant profile as it propagates. Reproduced with permission from ref. [41], copyright American Institute of Physics.

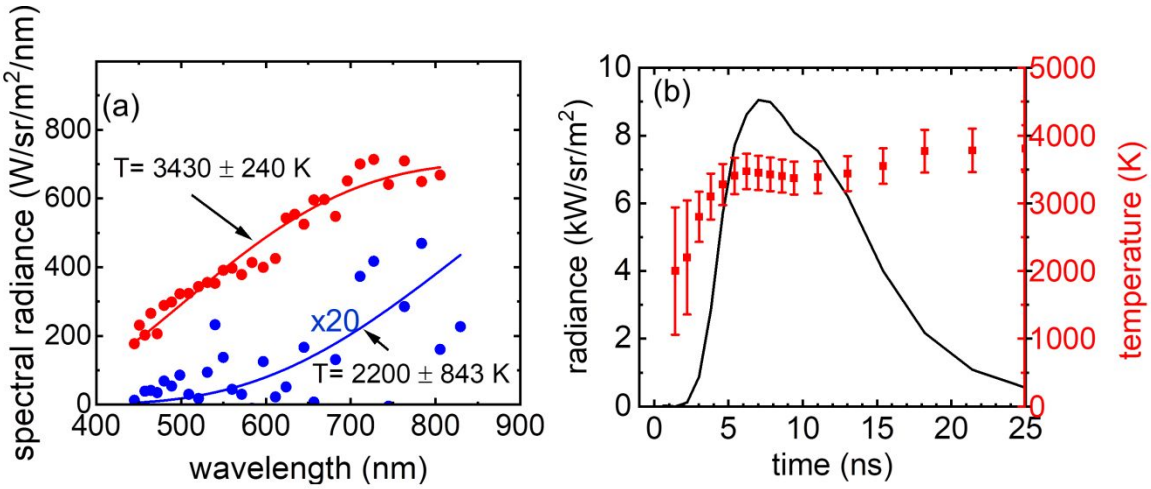

Fig. 12 (a) Spectral radiance at two times from shocked nitromethane along with temperatures deduced by fitting to a graybody model. (b) Time-dependent radiance and temperature profiles with a shock that produces a detonation around 10 ns. Reproduced with permission from ref. [41], copyright American Institute of Physics.

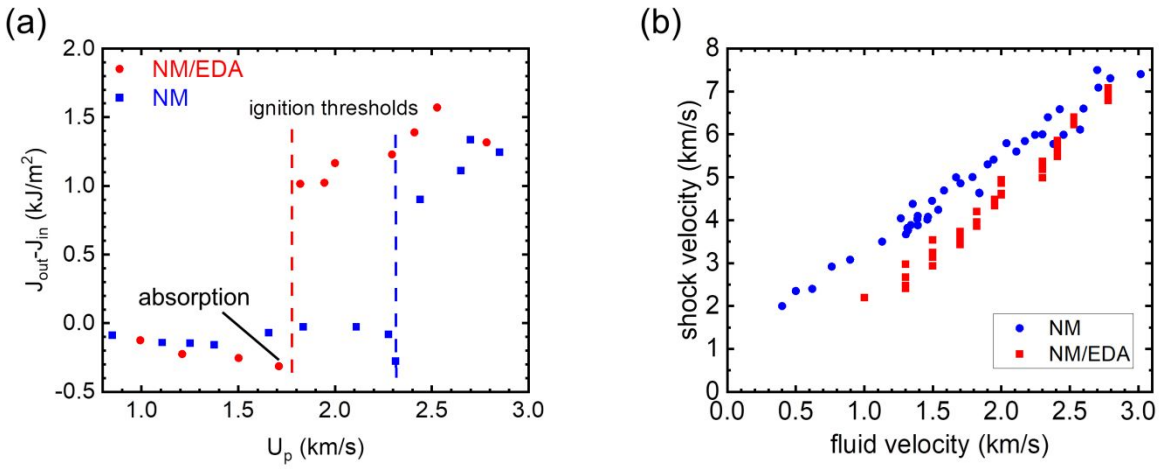

Fig. 13 A catalyst affects shocked nitromethane in two ways. (a) Adding EDA to NM lowers the threshold for shock energy absorption and ignition. (b) Adding EDA to NM reduces the shock velocity indicating a volume collapse that creates higher density and greater heating. Reproduced with permission from ref. [62], copyright American Chemical Society.

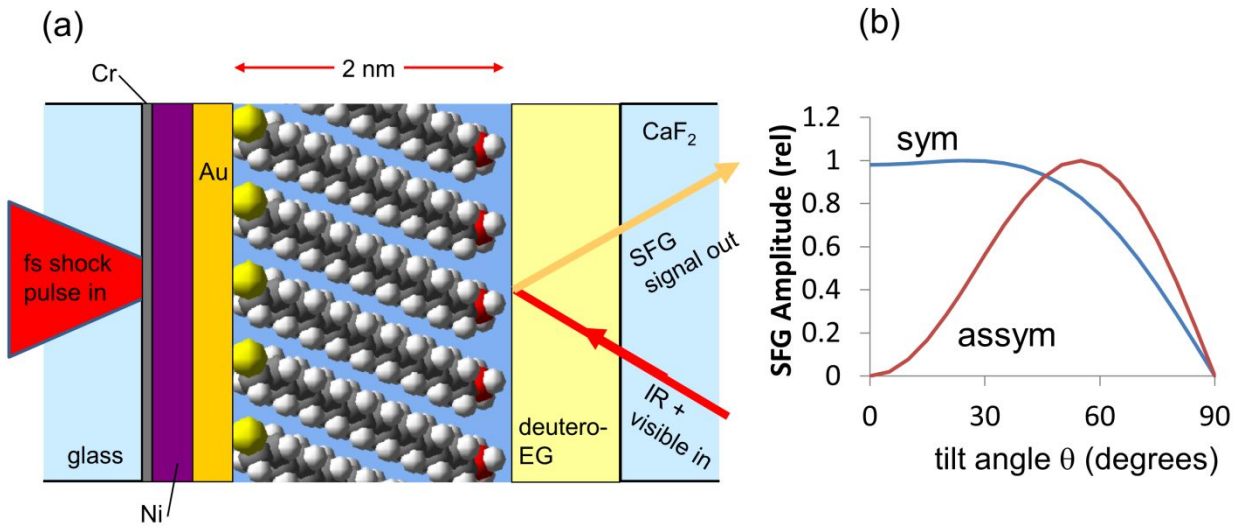

Fig. 14 Schematic of apparatus for watching a shock pass over a monolayer of methyl groups 1.5Å thick using vibrational sum-frequency generation (SFG). (b) The tilt angle of the methyl groups can be determined from the intensity ratio of symmetric to antisymmetric CH-stretch transitions. EG = ethylene glycol.

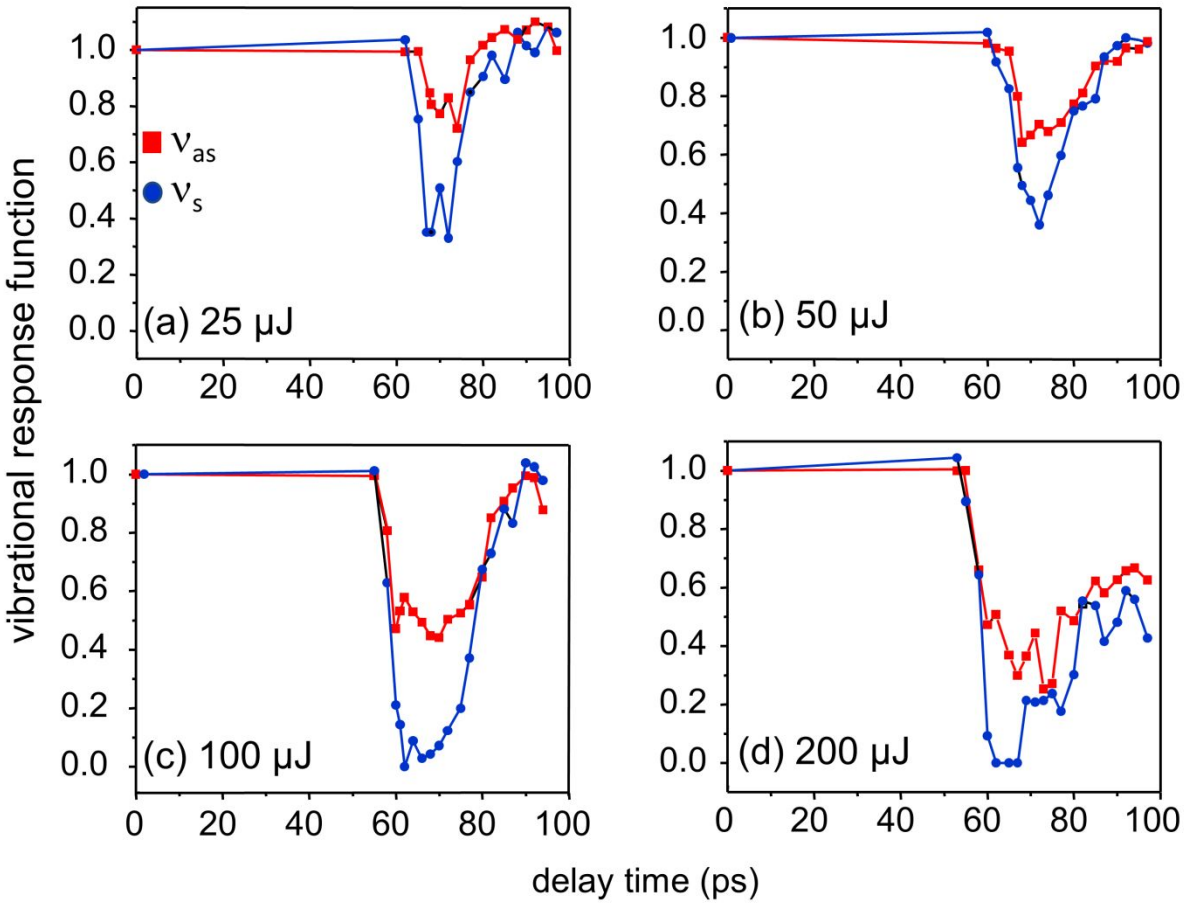

Fig. 15 Time-dependent SFG intensities for symmetric (s) and antisymmetric (as) CH-stretch transitions after shock up to 2 GPa. (a), (b), (c) The terminal methyl groups of the all-*trans* chains tilt reversibly but the recovery time increases with shock pressure. (d) The tilt becomes irreversible because the shock creates long-lived *gauche* defects in the chains.